GAMM-Mitt. **29**, No. 1, 9 – 28 (2006)

Modelling of terrestrial ice sheets in palaeo-climate research

Reinhard Calov[*1]

[1] Potsdam Institute for Climate Impact Research, PO Box 60 12 03, D-14412 Potsdam, Germany

Received 12 March 2005, revised 2 May 2005, accepted 17 May 2005

Key words shallow ice approximation, ice-sheet modelling, climate modelling, Last Glacial Inception, Heinrich events

This paper is dedicated to my mother Irmgard, deceased in September 27, 2004

The shallow ice equations are derived in spherical coordinates starting with the field equations and the constitutive law for terrestrial ice as a viscous heat conducting incompressible fluid. All these equations are expressed in spherical coordinates. Numerical representations of the shallow ice equations are implemented in a number of ice-sheet models. As applications of such a model in palaeo-climate research, simulations of the Last Glacial Inception and Heinrich events are shown. The polythermal ice-sheet model SICOPOLIS in its version coupled with the climate system model CLIMBER-2 is utilised for these simulations. The importance of the coupling of the ice sheets with the rest of the climate system is demonstrated. Further, the dependence of Heinrich events on the initial conditions is shown.

1 Introduction

By volume, the cryosphere is the third largest component of the climate system. Most of the present-day terrestrial ice is stored in the inland-ice masses of Greenland and Antarctica. The volume of the entire Antarctic ice sheet corresponds to about 60 m sea level and that of the Greenland ice sheet to roughly 7 m sea level [12]. While the East Antarctic ice sheet is certainly stable there is a debate whether the West Antarctic ice sheet might decay in the future, which could rise the sea level by about 5 m [3].

Several ice-sheet models have been developed during the last decades. Here, only the thermomechnical models will be discussed. Thermomechnical models treat the temporal variation of the shape of ice sheets as well as the evolution of temperature inside the ice. Knowledge of the temperature inside the ice is important, because the ice flow depends strongly on temperature. Furthermore, there are phenomena like Heinrich events (see below), which can be only understood if the development of ice temperature is computed. Certainly, this paper is not aimed to give a compilation of all ice-sheet models and their application. My only intention is to give an overview on the contemporary large-scale ice-sheet models.

* Corresponding author: e-mail: calov@pik-potsdam.de, Phone: +49 331 288 2595, Fax: +49 331 288 2570

The three dimensional (3D) ice-sheet model by Huybrechts [33] is based on a two dimensional (one vertical and one horizontal direction) pre-courser [35] and found several applications in modelling the Greenland and Antarctic ice sheets, palaeo ice sheet and in projections of future sea-level changes, e.g. [42, 37, 36, 34]. The model by Huybrechts includes ice shelves. These are large floating ice masses, which are fed by an ice sheet. The largest present-day ice shelves are the Filchner-Rønne and the Ross Ice Shelves in Antarctica. They play an important role for the stability of the West Antarctic ice sheet. Payne [49] developed a 2D thermomechanical ice-sheet model and used it to investigate internal oscillations of ice sheets (Heinrich events). Later the same author [51] introduced a 3D thermomechanical ice-sheet model. Among a number of other studies this 3D model was utilised to analyse ice stream formations in the Scandinavian ice sheet [50]. Ritz [53] investigated the sensitivity of the Greenland ice sheet to ice flow and ablation parameters. In another version of the model by Ritz ice shelves were included [54]. Further, the model was utilised to study different feedback mechanisms during the Last Glacial Inception [40]. The model by Marshall and Clarke [43] treats terrestrial ice as a mixture of slowly flowing ice sheets and more mobile ice streams. In their simulations of the Laurentide ice sheet [44] they found quasiperiodic surges of the ice in Hudson Strait associated with high ice-stream activity. The 3D thermomechanical ice-sheet model by Tarasov and Peltier [57] was used for simulations of the Last Glacial Cycle and, more recently, for an analysis of the deglacial history of the Laurentide ice sheet [58].

Here, two challenging phenomena of past climate changes are chosen to reveal the importance of the dynamics of ice sheets in palaeo-climate modelling; these are the Last Glacial Inception and Heinrich events. For an understanding of the future behaviour of the terrestrial ice sheets the investigation of past changes of the ice masses and an understanding of the mechanisms of past climate changes are vital.

The paper is organised as follows. First, a review is given of the field equations and the constitutive relations for terrestrial ice sheets as well as the basic equations of large-scale ice-sheet models are presented in Section 2. All equations are given in spherical coordinates. The numerical models used for the simulations are introduced in Section 3. In Section 4 results of simulations of the Last Glacial Inception and Heinrich events are presented. The concluding remarks in Section 5 close the paper.

2 The shallow ice approximation in spherical coordinates

Large-scale ice-sheet models, except those presented in [55] and [48], are based on the shallow ice approximation by [31, 47]. In climatology, ice sheets are often termed inland ice. I use both terms as synonyms. A review of the theory of the dynamics and thermodynamics of ice sheets can be found in [32, 9].

The spherical representation of the shallow ice equations is often used in ice-sheet models in their application in climate research. Spherical coordinates are convenient here, because the climate model, which the ice-sheet model is coupled to, is in spherical coordinates as well. Interpolation and downscaling procedures are easier to implement if the coordinates of the model components are of the same type. Therefore, the shallow ice equations are derived in spherical coordinates in this section.

2.1 Field equations

It is assumed that large ice masses behave as incompressible heat-conducting-nonlinear viscous fluids. This yields the balance equations

$$\begin{array}{lrcl} \text{mass:} & \boldsymbol{\nabla}\cdot\boldsymbol{v} & = & 0, \\ \text{energy:} & \rho\dot{u} & = & -\boldsymbol{\nabla}\cdot\boldsymbol{q} + \mathrm{tr}(\boldsymbol{t}^{\mathrm{D}}\boldsymbol{D}), \\ \text{momentum:} & \rho\dot{\boldsymbol{v}} & = & -\boldsymbol{\nabla}p + \boldsymbol{\nabla}\cdot\boldsymbol{t}^{\mathrm{D}} + \rho\boldsymbol{g}, \end{array} \tag{1}$$

and the constitutive relations

$$\boldsymbol{D} = EA(T')f(\sigma)\boldsymbol{t}^{\mathrm{D}}, \quad u = \int_{T_0}^{T} c_v(\bar{T})d\bar{T} + u_0, \quad \boldsymbol{q} = -\kappa(T)\nabla T, \tag{2}$$

where $\boldsymbol{v}$, p, $\boldsymbol{t}^{\mathrm{D}}$, ρ, $\boldsymbol{g}$, u, E, $\boldsymbol{D}$, T, $\boldsymbol{q}$, κ, c_v are, respectively, the velocity, pressure, stress deviator, density, gravity acceleration, internal energy, enhancement factor, strain rate tensor, temperature, heat flux vector, heat conductivity, and the specific heat at constant volume. The stress deviator is defined by

$$\boldsymbol{t}^{\mathrm{D}} = \boldsymbol{t} + p\,\mathbf{1}, \qquad p = -\tfrac{1}{3}\mathrm{tr}(\boldsymbol{t}), \tag{3}$$

where $\boldsymbol{t}$ and $\mathbf{1}$ are the stress tensor and the unit tensor, respectively. Furthermore, the homologous temperature T' is given by

$$T' = T + \beta p, \tag{4}$$

where β is the Clausius-Clapeyron constant. In most ice-sheet models, the temperature rate factor $A(T')$ is described by the Arrhenius relation

$$A(T') = A_0 \exp(-\frac{Q}{RT'}), \qquad T' \text{ in Kelvin} \tag{5}$$

where A_0 is a constant, $R = 8.314\,\mathrm{J\,mol^{-1}\,K^{-1}}$ is the universal gas constant and Q is the activation energy for creep. The fluidity is given by Glen's power law

$$f(\sigma) = \sigma^{n-1}\,, \tag{6}$$

with the effective shear stress

$$\sigma = \sqrt{\tfrac{1}{2}\mathrm{tr}(\boldsymbol{t}^{\mathrm{D}\,2})} = \sqrt{\tfrac{1}{2}\textstyle\sum_{i,j} t_{ij}^{\mathrm{D}} t_{ij}^{\mathrm{D}}}\,. \tag{7}$$

The transformation from Cartesian into spherical coordinates reads

$$\boldsymbol{x} = (x, y, z) = r(\cos\phi\cos\lambda, \cos\phi\sin\lambda, \sin\phi), \tag{8}$$

where r, ϕ and λ are the radial distance from the Earth's centre, the latitude and the longitude, respectively. Here, the latitude angle ϕ equals $\pm\pi$ at the poles. Applying (8) in the balance of mass $(1)_1$ leads to

$$\frac{1}{r^2}\frac{\partial}{\partial r}(r^2 v_r) + \frac{1}{r\cos\phi}\frac{\partial v_\lambda}{\partial\lambda} + \frac{1}{r\cos\phi}\frac{\partial}{\partial\phi}(\cos\phi\, v_\phi) = 0. \tag{9}$$

The spherical representation of the temperature evolution equation follows from equations $(1)_2$, (2),

$$\begin{aligned}&\frac{\partial T}{\partial t}+v_r\frac{\partial T}{\partial r}+\frac{v_\lambda}{r\cos\phi}\frac{\partial T}{\partial \lambda}+\frac{v_\phi}{r}\frac{\partial T}{\partial \phi}=\\&\frac{1}{\rho c(T)}\left(\frac{1}{r^2}\frac{\partial}{\partial r}(\kappa(T)r^2\frac{\partial T}{\partial r})+\frac{1}{r^2\cos^2\phi}\frac{\partial}{\partial\lambda}(\kappa(T)\frac{\partial T}{\partial\lambda}+\frac{1}{r^2\cos\phi}\frac{\partial}{\partial\phi}(\kappa(T)\cos\phi\frac{\partial T}{\partial\phi})\right)\\&+\frac{2}{\rho c(T)}EA(T')f(\sigma)\sigma^2.\end{aligned} \tag{10}$$

The momentum balance $(1)_3$ in spherical coordinates takes the form

$$\begin{aligned}\rho\frac{dv_r}{dt} &= -\frac{\partial p}{\partial r}+\frac{1}{r^2}\frac{\partial}{\partial r}(r^2t^{\mathrm{D}}_{rr})+\frac{1}{r\cos\phi}\frac{\partial t_{r\lambda}}{\partial\lambda}\\&\quad+\frac{1}{r\cos\phi}\frac{\partial}{\partial\phi}(\cos\phi\, t_{r\phi})-\frac{1}{r}(t^{\mathrm{D}}_{\lambda\lambda}+t^{\mathrm{D}}_{\phi\phi})-\rho g,\\ \rho\frac{dv_\lambda}{dt} &= -\frac{1}{r\cos\phi}\frac{\partial p}{\partial\lambda}+\frac{\partial t^{\mathrm{D}}_{\lambda\lambda}}{\partial r}+\frac{3}{r}t_{r\lambda}+\frac{1}{r\cos\phi}\frac{\partial t^{\mathrm{D}}_{\lambda\lambda}}{\partial\lambda}\\&\quad+\frac{1}{r}\frac{\partial t_{\lambda\phi}}{\partial\phi}-2\tan\phi\frac{t_{\lambda\phi}}{r},\\ \rho\frac{dv_\phi}{dt} &= -\frac{1}{r}\frac{\partial p}{\partial\phi}+\frac{\partial t_{r\phi}}{\partial r}+\frac{3}{r}t_{r\phi}+\frac{1}{r\cos\phi}\frac{\partial t_{\lambda\phi}}{\partial\lambda}\\&\quad+\frac{1}{r\cos\phi}\frac{\partial}{\partial\phi}(\cos\phi\, t^{\mathrm{D}}_{\phi\phi})+\frac{\tan\phi}{r}t^{\mathrm{D}}_{\lambda\lambda}.\end{aligned} \tag{11}$$

For the flow law of ice $(2)_1$ the transformation (8) yields

$$\begin{aligned}D_{r\lambda} &= \frac{1}{2}\left(r\frac{\partial}{\partial r}\left(\frac{v_\lambda}{r}\right)+\frac{1}{r\cos\phi}\frac{\partial v_r}{\partial\lambda}\right) &&= 2EA(T')f(\sigma)t_{r\lambda},\\ D_{r\phi} &= \frac{1}{2}\left(r\frac{\partial}{\partial r}\left(\frac{v_\phi}{r}\right)+\frac{1}{r}\frac{\partial v_r}{\partial\phi}\right) &&= 2EA(T')f(\sigma)t_{r\phi}.\end{aligned} \tag{12}$$

In what follows the other four components of $(2)_1$ are not required and therefore not listed here.

2.2 Introduction of scales

In order to derive the shallow ice equations in spherical coordinates I now introduce the scalings

$$\begin{aligned}\{r,\ \lambda,\ \phi,\ t\} &= \{[r_0]\tilde{r_0}+[H]\tilde{r},\ [\mathcal{L}]\tilde{\lambda},\ [\mathcal{L}]\tilde{\phi},\ \tfrac{[r_0][\mathcal{L}]}{[v_H]}\tilde{t}\},\\ \{v_r,\ v_\lambda,\ v_\phi\} &= \{[v_r]\tilde{v}_r,\ [v_H]\tilde{v}_\lambda,\ [v_H]\tilde{v}_\phi\},\\ \{p,\ t_{r\lambda},\ t_{r\phi},\ \sigma\} &= \rho g[H]\{\tilde{p},\ \epsilon\tilde{t}_{r\lambda},\ \epsilon\tilde{t}_{r\phi},\ \epsilon\tilde{\sigma}\},\\ \{t^{\mathrm{D}}_{rr},\ t^{\mathrm{D}}_{\lambda\lambda},\ t^{\mathrm{D}}_{\phi\phi},\ t_{\lambda\phi}\} &= \rho g[H]\epsilon^2\{\tilde{t}^{\mathrm{D}}_{rr},\ \tilde{t}^{\mathrm{D}}_{\lambda\lambda},\ \tilde{t}^{\mathrm{D}}_{\phi\phi},\ \tilde{t}_{\lambda\phi}\},\\ \{T,\ c(T),\ \kappa(T)\} &= \{[\Delta T]\tilde{T},\ [c]\tilde{c}(\tilde{T}),\ [\kappa_0]\tilde{\kappa}_0+[\Delta\kappa]\tilde{\kappa}(\tilde{T})\},\\ \{A(T'),\ f(\sigma)\} &= \{[A]\tilde{A}(\tilde{T'}),\ [f]\tilde{f}(\tilde{\sigma})\},\end{aligned} \tag{13}$$

where $[r_0]$, $[H]$, $[\mathcal{L}]$, $[v_H]$, $[v_r]$, $[\Delta T]$, $[c]$, $[\kappa_0]$, $[\Delta\kappa]$, $[A]$ and $[f]$ are typical values for the Earth's radius, the ice thickness, the angles of the spherical coordinates (in radiant), the absolute value of the horizontal velocity $\boldsymbol{v}_H$, the vertical velocity, the temperature range, the specific heat of ice, the heat-conductivity offset, the absolute heat conductivity, the rate factor and the fluidity. These typical values are chosen such that the dimensionless model variables, which are indicated by tildes, are of order unity. The relations $(13)_{3,4}$ have originally been suggested by Greve [23]. Substitution of the scalings (13) into the spherical field equations (9) to (12) leads to the dimensionless products

$$\begin{aligned} \epsilon &= \frac{[H]}{[r_0][\mathcal{L}]} = \frac{[v_r]}{[v_H]}, \quad [\mathcal{L}], \quad \mathcal{F} = \frac{[v_H]^2}{g[r_0][\mathcal{L}]}, \\ \mathcal{D} &= \frac{[\kappa_0]}{\rho[c][H][v_r]}, \quad \alpha = \frac{g[H]}{[c][\Delta T]}, \quad \psi = \frac{[\Delta\kappa]}{[\kappa_0]}, \quad \mathcal{K} = \frac{\rho g[H]^3[A][f]}{[\mathcal{L}][r_0][v_H]}, \end{aligned} \tag{14}$$

where ϵ, $\mathcal{F}$, $\mathcal{D}$, α, ψ, and $\mathcal{K}$ are called aspect ratio, Froude number, thermal diffusivity number, ratio of the potential energy to the internal energy, ratio of the heat-conductivity offset to the absolute heat conductivity and fluidity number. Note that $[\mathcal{L}]$ itself is dimensionless. The scalings (13) and the dimensionless products (14) are as in the Cartesian case, except for the vertical direction r (measured from the Earth's centre) and the angles (λ, ϕ). The vertical offset $[r_0]$ has to be introduced to reach a simple representation of the derivatives with respect to $\tilde{r}$, as it will be shown later. A typical value $[\mathcal{L}]$ for the angles ensures the validity of the spherical shallow ice approximation for small as well as for large ice sheets. If it is assumed that $[\mathcal{L}]$ is an arbitrary angle on the Earth's surface (considered as a sphere), one can express the typical horizontal extension as $[L] = [\mathcal{L}][r_0]$. This yields for the aspect ratio

$$\epsilon = \frac{[H]}{[L]}, \tag{15}$$

which elucidates the connection to the shallow ice approximation in Cartesian coordinates [32, 9]. The choice of $[\mathcal{L}]$ determines whether ice sheets with small or large horizontal extensions are considered. The typical ice thickness $[H]$ over the typical horizontal extension $[L]$ gives with (15) the well known aspect ratio. For the Greenland ice sheet ($[\mathcal{L}] \approx 0.3$, $[H] \approx 3$ km) it follows $[L] \approx 2000$ km and $\epsilon \approx 0.0015$.

In what follows the scaled variables are introduced in the spherical field equations (9) to (12). Note that in the equations below all variables are dimensionless, and the corresponding tildes are omitted for simplicity.

- Mass balance

$$\begin{aligned} \frac{1}{(r_0+\epsilon[\mathcal{L}]r)^2}\frac{\partial}{\partial r}\left((r_0+\epsilon[\mathcal{L}]r)^2 v_r\right) &+ \frac{1}{(r_0+\epsilon[\mathcal{L}]r)\cos\phi}\frac{\partial v_\lambda}{\partial\lambda} \\ &+ \frac{1}{(r_0+\epsilon[\mathcal{L}]r)\cos\phi}\frac{\partial}{\partial\phi}\left(\cos\phi\, v_\phi\right) = 0. \end{aligned} \tag{16}$$

- Temperature equation

$$\begin{aligned}
&\frac{\partial T}{\partial t} + v_r \frac{\partial T}{\partial r} + \frac{v_\lambda}{(r_0+\epsilon[\mathcal{L}]r)\cos\phi}\frac{\partial T}{\partial \lambda} + \frac{v_\phi}{r_0+\epsilon[\mathcal{L}]r}\frac{\partial T}{\partial \phi} = \\
&\frac{\mathcal{D}}{c(T)}\left\{\frac{1}{(r_0+r)^2}\frac{\partial}{\partial r}\left((\kappa_0+\psi\kappa(T))(r_0+\epsilon[\mathcal{L}]r)^2\frac{\partial T}{\partial r}\right)\right. \\
&+\frac{\epsilon^2}{(r_0+\epsilon[\mathcal{L}]r)^2\cos^2\phi}\frac{\partial}{\partial \lambda}\left((\kappa_0+\psi\kappa(T))\frac{\partial T}{\partial \lambda}\right) \\
&\left.+\frac{\epsilon^2}{(r_0+\epsilon[\mathcal{L}]r)^2\cos\phi}\frac{\partial}{\partial \phi}\left((\kappa_0+\psi\kappa(T))\cos\phi\frac{\partial T}{\partial \phi}\right)\right\} + \frac{2\alpha\mathcal{K}EA(T')}{\rho c(T)} f(\sigma)\sigma^2.
\end{aligned} \tag{17}$$

- Momentum balance

$$\begin{aligned}
\epsilon\mathcal{F}\frac{dv_r}{dt} &= -\frac{\partial p}{\partial r} + \frac{\epsilon^2}{(r_0+\epsilon[\mathcal{L}]r)^2}\frac{\partial}{\partial r}((r_0+\epsilon[\mathcal{L}]r)^2 t^{\mathrm{D}}_{rr}) + \frac{\epsilon^2}{(r_0+\epsilon[\mathcal{L}]r)\cos\phi}\frac{\partial t_{r\lambda}}{\partial \lambda} \\
&+ \frac{\epsilon^2}{(r_0+\epsilon[\mathcal{L}]r)\cos\phi}\frac{\partial}{\partial \phi}(\cos\phi\, t_{r\phi}) - \frac{\epsilon^3[\mathcal{L}]}{r_0+\epsilon[\mathcal{L}]r}(t^{\mathrm{D}}_{\lambda\lambda} + t^{\mathrm{D}}_{\phi\phi}) - 1, \\
\frac{\mathcal{F}}{\epsilon}\frac{\partial v_\lambda}{\partial t} &= -\frac{1}{(r_0+\epsilon[\mathcal{L}]r)\cos\phi}\frac{\partial p}{\partial \lambda} + \frac{\partial t_{r\lambda}}{\partial r} + \frac{3\epsilon[\mathcal{L}]}{r_0+\epsilon[\mathcal{L}]r}t_{r\lambda} \\
&+ \frac{\epsilon^2}{(r_0+\epsilon[\mathcal{L}]r)\cos\phi}\frac{\partial t^{\mathrm{D}}_{\lambda\lambda}}{\partial \lambda} + \frac{\epsilon^2}{r_0+\epsilon[\mathcal{L}]r}\frac{\partial t_{\lambda\phi}}{\partial \phi} - \frac{2\epsilon^2[\mathcal{L}]\tan\phi}{r_0+\epsilon[\mathcal{L}]r}t_{\lambda\phi}, \\
\frac{\mathcal{F}}{\epsilon}\frac{\partial v_\phi}{\partial t} &= -\frac{1}{r_0+\epsilon[\mathcal{L}]r}\frac{\partial p}{\partial \phi} + \frac{\partial t_{r\phi}}{\partial r} + \frac{3\epsilon[\mathcal{L}]}{r_0+\epsilon[\mathcal{L}]r}t_{r\phi} + \frac{\epsilon^2}{(r_0+\epsilon[\mathcal{L}]r)\cos\phi}\frac{\partial t_{\lambda\phi}}{\partial \lambda} \\
&+ \frac{\epsilon^2}{(r_0+\epsilon[\mathcal{L}]r)\cos\phi}\frac{\partial}{\partial \phi}(\cos\phi\, t^{\mathrm{D}}_{\phi\phi}) + \frac{\epsilon^2[\mathcal{L}]\tan\phi}{r_0+\epsilon[\mathcal{L}]r}t^{\mathrm{D}}_{\lambda\lambda}.
\end{aligned} \tag{18}$$

- Flow law of ice

$$\begin{aligned}
(r_0+\epsilon[\mathcal{L}]r)\frac{\partial}{\partial r}\left(\frac{v_\lambda}{r_0+\epsilon[\mathcal{L}]r}\right) + \frac{\epsilon^2}{(r_0+\epsilon[\mathcal{L}]r)\cos\phi}\frac{\partial v_r}{\partial \lambda} &= 2\mathcal{K}AEf(\sigma)t_{r\lambda}, \\
(r_0+\epsilon[\mathcal{L}]r)\frac{\partial}{\partial r}\left(\frac{v_\phi}{r_0+\epsilon[\mathcal{L}]r}\right) + \frac{\epsilon^2}{r_0+\epsilon[\mathcal{L}]r}\frac{\partial v_r}{\partial \phi} &= 2\mathcal{K}AEf(\sigma)t_{r\phi}.
\end{aligned} \tag{19}$$

The derivative with respect to r in the scaled mass balance (16) takes for small ϵ the limit

$$\lim_{\epsilon\to 0}\frac{1}{(r_0+\epsilon[\mathcal{L}]r)^2}\frac{\partial}{\partial r}\left((r_0+\epsilon[\mathcal{L}]r)^2 v_r\right) = \frac{\partial v_r}{\partial r}, \tag{20}$$

because the vertical direction is large compared with its variation. Analogous approximations can also be performed for the heat equation (17) and the flow law (19) reducing the computational time in the numerical procedure. While the scaled momentum balance in Cartesian

coordinates contains no terms of order $\mathcal{O}(\epsilon)$, the stress tensor components $t_{r\lambda}$ and $t_{r\phi}$ in equations $(18)_{2,3}$ possess such terms.

The scaled effective shear stress (7) reads

$$\sigma = \sqrt{t_{r\lambda}^2 + t_{r\phi}^2 + \frac{\epsilon^2}{2}(t^{\mathrm{D}}{}_{rr}^2 + t^{\mathrm{D}}{}_{\lambda\lambda}^2 + t^{\mathrm{D}}{}_{\phi\phi}^2 + 2t_{\lambda\phi}^2)} \tag{21}$$

This result is analogous to the Cartesian case.

2.3 The shallow ice equations

Neglecting the terms with ϵ and $\mathcal{F}$ leads to a reduced model, the shallow ice approximation. The limits

$$\mathcal{F} \to 0, \quad \mathcal{F}/\epsilon \to 0, \quad \epsilon \to 0, \tag{22}$$

are performed, and the system of equations is transformed back to the dimensional notation, which yields the reduced model equations. In what follows the variables without tildes denote again the dimensional quantities.

Thus, the ice-thickness evolution equation[1] follows from equation (16),

$$\frac{\partial H}{\partial t} = -\boldsymbol{\nabla}_H^{r_0} \cdot \boldsymbol{Q} + M + M^*, \quad \boldsymbol{Q} = \int_b^h \boldsymbol{v}_H \, dr, \tag{23}$$

where H, h, b, $\boldsymbol{Q}$, $\boldsymbol{v}_H$, M and M^* are the ice thickness, surface elevation, bottom altitude, mass (better: volume) flux, horizontal velocity ($\boldsymbol{v}_H = \hat{\boldsymbol{e}}_\lambda v_\lambda + \hat{\boldsymbol{e}}_\phi v_\phi$), accumulation-ablation rate[2] (snowfall minus melting) and basal melting of the ice sheet, respectively. The horizontal spherical divergence is given by

$$\boldsymbol{\nabla}_H^{r_0} \cdot \boldsymbol{Q} = \frac{1}{r_0 \cos\phi} \frac{\partial Q_\lambda}{\partial \lambda} + \frac{1}{r_0 \cos\phi} \frac{\partial}{\partial \phi}(\cos\phi \, Q_\phi), \tag{24}$$

and the reduced temperature evolution equation reads

$$\frac{\partial T}{\partial t} + v_r \frac{\partial T}{\partial r} + \frac{v_\lambda}{r_0 \cos\phi} \frac{\partial T}{\partial \lambda} + \frac{v_\phi}{r_0} \frac{\partial T}{\partial \phi} = \frac{1}{\rho c(T)} \frac{\partial}{\partial r}(\kappa(T(r)) \frac{\partial T}{\partial r}) + 2EA(T')f(\sigma)\sigma^2. \tag{25}$$

Note that in equation (25) the heat conductivity $\kappa(T(r))$ is differentiated with respect to the vertical direction r. This is so, because the heat conductivity is temperature-dependent, and the ice temperature varies conspicuously in the vertical direction.

The reduced momentum balance is

$$\frac{\partial p}{\partial r} + \rho g = 0, \quad \frac{1}{r_0 \cos\phi} \frac{\partial p}{\partial \lambda} - \frac{\partial t_{r\lambda}}{\partial r} = 0, \quad \frac{1}{r_0} \frac{\partial p}{\partial \phi} - \frac{\partial t_{r\phi}}{\partial r} = 0, \tag{26}$$

[1] To derive the ice-thickness evolution equation the kinematic conditions at the free surface and the base of the ice sheet must apply. Since this is analogous to the Cartesian case, it is not demonstrated here.

[2] In glaciology the "accumulation-ablation rate" is called mass balance; we avoid it in order not to confuse it with the balance of mass

and the reduced flow law is given by

$$\frac{\partial \boldsymbol{v}_H}{\partial r} = 2EA(T')f(\sigma)\boldsymbol{\tau}_H, \quad \text{with} \quad \boldsymbol{\tau}_H := t_{r\lambda}\hat{\boldsymbol{e}}_\lambda + t_{r\phi}\hat{\boldsymbol{e}}_\phi. \tag{27}$$

The reduced momentum balance (26) is similar to that in Cartesian coordinates. Without the coefficients $1/(r_0 \cos\phi)$ and $1/r_0$ equation (26) would have the same form as in Cartesian coordinates. The reduced effective shear stress follows from (21) and reads

$$\sigma = \sqrt{t_{r\lambda}^2 + t_{r\phi}^2} = \rho g(h-r) \parallel \boldsymbol{\nabla}_H^{r_0} h \parallel, \tag{28}$$

with the definitions

$$\boldsymbol{\nabla}_H^{r_0} h = \frac{1}{r_0 \cos\phi}\frac{\partial h}{\partial \lambda}\hat{\boldsymbol{e}}_\lambda + \frac{1}{r_0}\frac{\partial h}{\partial \phi}\hat{\boldsymbol{e}}_\phi, \quad \parallel \boldsymbol{\nabla}_H^{r_0} h \parallel = \sqrt{\frac{1}{r_0^2\cos^2\phi}\left(\frac{\partial h}{\partial \lambda}\right)^2 + \frac{1}{r_0^2}\left(\frac{\partial h}{\partial \phi}\right)^2}. \tag{29}$$

Because the Earth's radius r_0 is constant in our approximation, the system of differential equations (26) and (27) can be integrated analogously to the Cartesian case. Before doing this, let me introduce the boundary conditions at the ice surface $r = h(\lambda, \phi, t)$ the stress free conditions

$$p = 0, \qquad t_{r\lambda} = t_{r\phi} = 0, \tag{30}$$

and at the bottom of the ice sheet $r = b(\lambda, \phi, t)$ the nonlinear viscous sliding law

$$\boldsymbol{v}_H(b) = -c_s(\rho g H)^{m-l} \parallel \boldsymbol{\nabla}_H^{r_0} h \parallel^{m-1} \boldsymbol{\nabla}_H^{r_0} h, \tag{31}$$

where c_s, l and m are parameters which will be fixed later.

Together with the boundary conditions (30) the reduced momentum balance equations (26) in integrated form yield

$$p = \rho g(h-r), \quad \boldsymbol{\tau}_H = -\rho g(h-r)\boldsymbol{\nabla}_H^{r_0} h. \tag{32}$$

Substitution of $(32)_2$ into the flow law components $(27)_1$ leads to

$$\boldsymbol{v}_H(r, \lambda, \phi, t) = \boldsymbol{v}_H(b) + C(r, t, \parallel \boldsymbol{\nabla}_H^{r_0} h \parallel)\, \boldsymbol{\nabla}_H^{r_0} h, \tag{33}$$

with

$$C(r, t, \parallel \boldsymbol{\nabla}_H^{r_0} h \parallel) = -2\rho g \int_b^r EA(T'(r'))\, f(\rho g \parallel \boldsymbol{\nabla}_H^{r_0} h \parallel (h-r'))(h-r')\, dr'. \tag{34}$$

The vertical velocity follows in a subsequent step from the scaled mass balance

$$v_r = v_r(b) - \int_b^r \boldsymbol{\nabla}_H^{r_0} \cdot \boldsymbol{v}_H \, dr'. \tag{35}$$

Equations (23), (28), (31) and (32) to (35) are analogous to the corresponding Cartesian equations. It should be admitted that these results could also be found heuristically. Nevertheless, a proper scaling shows the limits of the validity of the theory. Additionally, the spherical representations of the shallow ice equations presented above can be useful for further theoretical considerations.

3 The models

A version of the polythermal ice-sheet model SICOPOLIS has been included into the climate-system model CLIMBER-2. On time scales longer than about 5000 years, the cryosphere becomes an important part of the climate system. The cryosphere is coupled with the atmosphere and the ocean. The surface temperature and the accumulation-ablation rate (snowfall minus melting) alter the shape of the ice sheet and the temperature in the ice-sheet. Vice versa, inland ice feeds back to the atmosphere by the ice surface elevation and albedo; similarly the ocean acts in this system by its fresh water fluxes.

In addition to other ice-sheet models, SICOPOLIS differentiates between regions of cold ice, i.e. ice below the melting point, and warm or temperate ice, i.e. ice at the melting point. The respective equations are not shown in Section 2; their Cartesian form is derived in [24].

3.1 The climate-system model CLIMBER-2

CLIMBER-2 is an Earth System Model of Intermediate Complexity (EMIC); see [14] for a comprehensive description of the contemporary EMICs. Such kinds of models provide the only chance to simulate the behaviour of the climate system over longer time scales while having, at the same time, still the most important climate components integrated (atmosphere, ocean, terrestrial vegetation, inland ice) in the model with sufficient details of description. CLIMBER-2, was designed for simulations lasting between 10 years and up to 1,000,000 years.

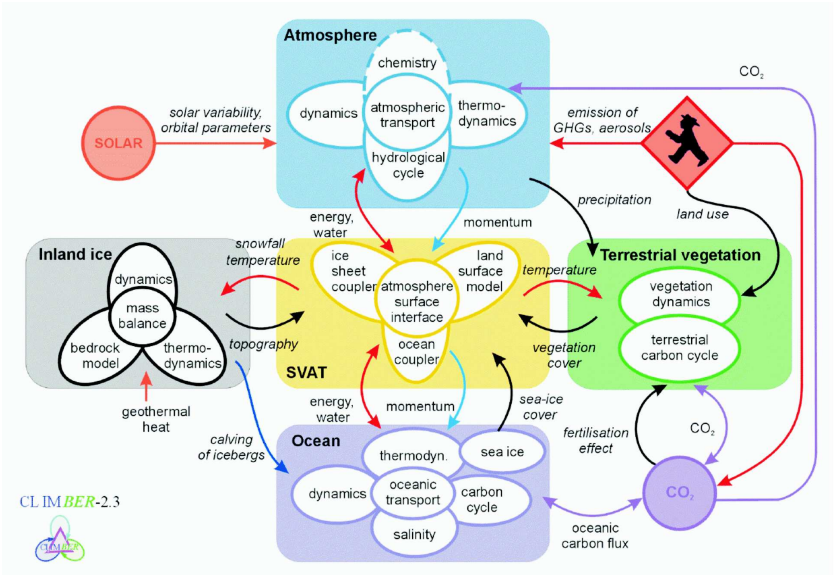

Fig. 1 Block diagram of the components of Climber-2 (version 3). Sketch by Andrey Ganopolski. The inland ice (or synonymous the ice sheets) is represented by the polythermal ice-sheet model SICOPOLIS

For even longer simulation times so-called conceptual models with a lower grade of description as EMICs are more appropriate. Fig. 1 illustrates with a block diagram the models components of CLIMBER-2.

The atmospheric part of CLIMBER-2 is a statistical dynamic model, which was developed by [52]. It has a resolution of 51° in longitude and 10° in latitude. The ocean module consists of three basins representing the Pacific, Atlantic and Indian Oceans and is described by a model of the Stocker-Wright type [56]. Each basin is resolved with 2.5° in latitude and has 20 unequally thick layers in the vertical direction. The vegetation module treats different types of plants and their CO_2 storage [5]. Fig. 1, shows the quantities which determine the various components of CLIMBER-2 and it illustrates the couplings between the different modules.

CLIMBER-2 has been used for a variety of dynamical studies including those of the Holocene [20] the Last Glacial Maximum [21], Dansgaard-Oeschger Oscillations [22] and Heinrich Events [8]. Dansgaard-Oeschger Oscillations are rapid past climate changes during the mid and late part of the last glaciation. Phases of relatively mild climate conditions (interstadials) punctuated the cold background climate about every 1500 to 3000 years. Evidence for these oscillations are found in data (so-called proxy-data; climate change of the farer past can be measured indirectly only) of Greenland ice cores as well as marine cores [15, 4]. Heinrich events mostly appear in the later half of a glacial cycle [45]. Further discussions about Heinrich events can be found in section 4.2. Both Dansgaard-Oeschger Oscillations and Heinrich Events are associated with changes in the circulations of the Atlantic Ocean [13].

3.2 The polythermal ice-sheet model SICOPOLIS

As an example for a state-of-the-art ice-sheet model, the polythermal ice-sheet model SICOPOLIS is described here. In principle, all 3D thermomechanical ice-sheet models are capable to represent the cryosphere in CLIMBER-2. SICOPOLIS [24, 25] calculates three-dimensionally the temporal evolution of the ice extent, thickness, velocity, temperature, water content and age. The model found numerous applications to past and future ice masses on Earth or on Mars, e.g. [25, 10, 26, 18, 17].

In SICOPOLIS, temperate ice is treated as a binary mixture of warm ice and a small component water amounting up to 1 %. The interface that separates cold and temperate ice is monitored through the use of Stefan-type energy flux and mass flux matching conditions. The accordant equations are not show in Section 2 but their derivation follow the same spirit. The response of the lithosphere and asthenosphere to the changing load due to the evolving ice sheets is treated by a simple local relaxation-type model with an isostatic time lag of $\tau_{\rm V} = 3\,{\rm kyr}$. A detailed description of SICOPOLIS can be found in [23, 24].

SICOPOLIS, has further the option to change coordinate systems in which the model is run. For the model version of SICOPOLIS which is coupled to the climate-system models CLIMBER-2 the spherical representation of the ice-sheet equations are used. In these studies, SICOPOLIS is operated on a resolution of 1.5° in longitude and 0.75° in latitude. The vertical direction is subdivided into 21 levels independent of the ice thickness and with decreasing layer thickness with depth in the ice. For further details concerning the setup see [6]

3.3 Coupling

Because SICOPOLIS and CLIMBER-2 have a different resolution a coupling and downscaling procedure is implemented. SICOPOLIS provides CLIMBER-2 with the temporal change of surface elevation and the distribution of land area and inland-ice area, which are aggregated on the coarse grid. Conversely, the climate characteristics (air temperature and humidity, long-wave and short-wave radiation, precipitation), calculated by CLIMBER-2 on the coarse grid, are utilised to compute the energy balance and the accumulation-ablation rate on the fine grid of SICOPOLIS. The coupling procedure is rather sophisticated, e.g. the precipitation downscaling accounts for orography effects of the fine grid. Details of the coupling are given in [6].

4 Application of an ice-sheet model in palaeo-climate modelling

4.1 Last Glacial Inception

Glacial inceptions are rapid, on geological timescales, glaciations of the Earth's surface during the Earth's history. During the Quaternary, such glaciations happened relatively often on the Northern Hemisphere and find evidence in several sources, e.g. [16]. The build-up and decay of the inland ice led to changes of sea level. During the Last Glacial Maximum (21 kyr BP, 21,000 years before present) the sea level was about 120 m lower than at present-day. Fig. 2 shows the sea-level change through the last 800,000 years derived from a variety of marine cores known as the already classical SPECMAP curve.

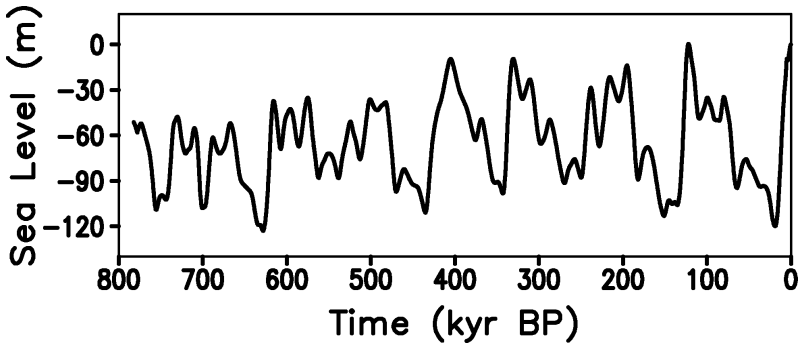

Fig. 2 Sea level change in m from the marine SPECMAP cores [38]. The Last Glacial Cycle from 125 kyr BP to present-day is clearly seen

Today it is generally accepted that glacial inceptions are caused by long-term changes of the Earth's orbital parameters (precession, obliquity, eccentricity), which lead to a change of the radiation at the top of the Earth's atmosphere. This radiation is commonly named insolation. After Milankovitch [46] the summer insolation ("caloric summer half year") is important; snow which was accumulated in a preceding winter has less tendency to be molten in a rather long and cold succeeding summer. The climate system can amplify the effect of a drop of summer insolation [2].

Simulations of the Last Glacial Inception using an EMIC including ice sheets have been done before by [60, 40]. Model studies by [6] explained glacial inception as a bifurcation in

the climate system caused by a strong snow albedo feedback when the summer insolation is dropping. Other components in the climate system like vegetation via southward retreat of boreal forest and the ocean via expansion of sea ice amplify the Last Glacial Inception [7].

The simulation presented in the following is fully coupled, i.e., all model components (atmosphere, vegetation, ocean and inland ice) can interact with each other. The only external forcings are the latitudinal and seasonally varying insolation and the CO_2 content of the atmosphere. The latter is prescribed from data after [1]. The model is run for 26,000 years starting at the last interglacial (the Eemian, 126 kyr BP) with the climate conditions at that time. Because the Eemian expansion of the ice sheets is rather unknown, the present-day equilibrium distribution in shape and temperature of the Greenland ice sheet is taken as initial condition for the ice sheets. See [6] for details.

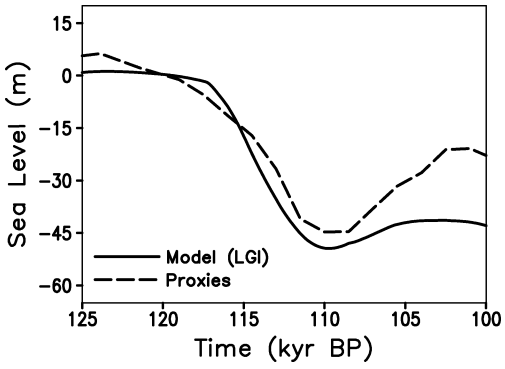

Fig. 3 Modelled-sea level change (solid line) in comparison with marine data by [59] (dashed line). The sea levels are in m

Fig. 3 shows the simulated sea-level change in comparison with proxy-data by [59]. At about 117 kyr BP, the sea level starts to drop rapidly. The sea level drops by 50 m in less than 10,000 years, which corresponds well with the proxy-data. After 110 kyr BP the sea level starts to rise again, but not as intensely as in the observation. The reason for this might be that the ice in the model is not mobile enough.

Fig. 4 shows time series of surface elevation of the ice sheets on the Northern Hemisphere. The simulation has been started at the previous interglacial (the Eemian, 126 kyr BP) with the modelled present-day equilibrium ice sheets (Fig. 4a). The ice first developed over Baffin Island, northern Quebec and parts of the Canadian Archipelago (Fig. 4b). Figs. 4b,c,d illustrate that the ice first grows rapidly in area with the ice volume following slowly thereafter. This behaviour is different from the traditional view of glacial inception as a slow growth of ice caps from small nucleation centres [16, 61]. Such a growth cannot explain the rapidity of the drop in sea level during the Last Glacial Inception as indicated in the palaeo records. A more appropriate concept, the "instantaneous glaciation", was discussed by [39]. The simulations of this paper rather support such a concept. In should be noted that such a fast glaciation in area never could be simulated with an ice-sheet-only model, because the feedback mechanism of the climate system are very important here. See [6] for details.

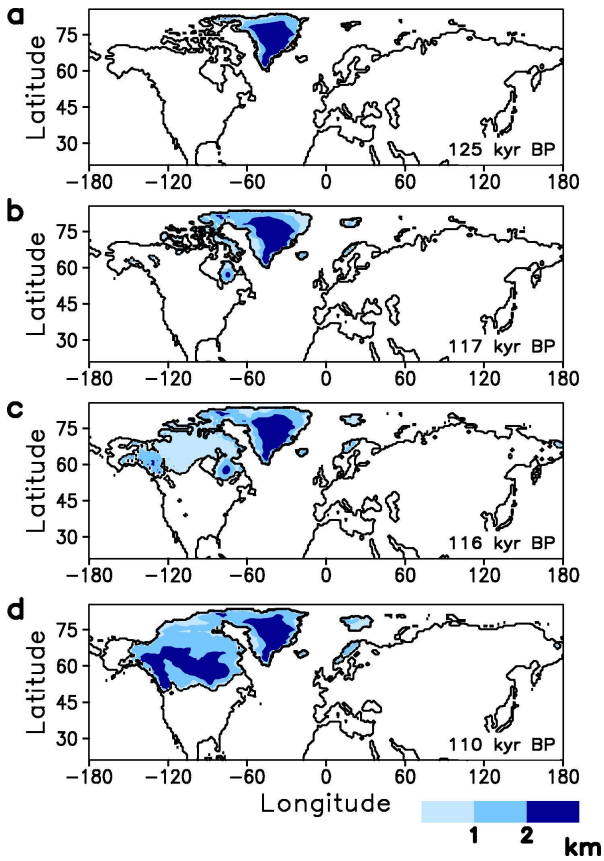

Fig. 4 Time series of elevation of ice sheets in km on the Northern Hemisphere during Last Glacial Inception. (**a**) elevation at 125 kyr BP, (**b**) 117 kyr BP, (**c**) 116 kyr BP and (**d**) 110 kyr BP

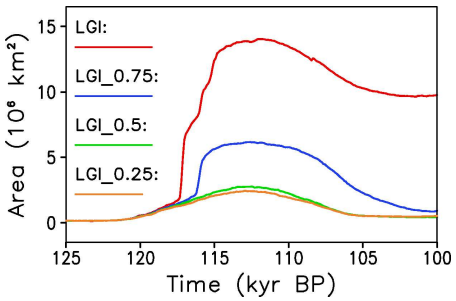

Fig. 5 Time series of ice area in 10^6 km^2 during last glacial for different simulations. Explanation see text

Here, the importance of the coupling of the ice sheets with the remainder of the climate system is demonstrated directly (Fig. 5). The impact of change in vegetation, the ocean and

the CO_2 content of the atmosphere on the Earth's surface ice cover was investigated by [7] in greater detail. The simulations of the Last Glacial Inception in this paper are denoted with the acronym "LGI". Simulation LGI is fully coupled; i.e. all simulated components of the climate system (atmosphere, vegetation, ocean, inland ice; see Fig. 1) can interact with each other. However, in simulations LGI_0.25, LGI_0.5 and LGI_0.75 the ice area passed to the climate module is reduced by a damping factor of 0.25, 0.5 and 0.75, respectively. The evolution of ice area in simulation LGI once more illustrates the rapidity of the increase of ice area at about 117 kyr BP. One can also see that the damping factor owns a threshold: If the damping factor is decreased from 1 to 0.75 or from 0.75 to 0.5 the maximum ice volume decreases in both cases. But further decrease leads to minor response in ice area only. The ice area in simulation LGI_0 (damping factor zero, not shown here) is practically identical with that from simulation LGI_0.25. This behaviour can be explained with the successive reduction of the snow albedo feedback through the introduced decrease of the damping factor in the considered simulations. It is also a strong hint that there are two equilibria in the climate-cryosphere system: an interglacial state and a glacial state. The proof of this, if one accepts numerical simulations as a proof, was given in [6].

4.2 Heinrich Events

Heinrich events are large-scale surges from the Laurentide ice sheet during glacial times. They appear if the basal ice over the Hudson Bay and Hudson Strait reaches the melting point and begins to slide rapidly over the soft sediment there. Material (so-called ice rafted detritus) from that provenance and carried by icebergs was found in marine cores in the North Atlantic [29]. Heinrich events belong to the most interesting phenomena in the climate system. During a Heinrich event sea level rose by several meters in some hundred years and the thermohaline circulation in the Atlantic broke down leading to substantial cooling in a broad region around the North Atlantic.

Self-sustained oscillations like Heinrich events were modelled before with 2D ice-sheet models (one vertical and one horizontal direction) by [49, 27, 30]. With a 3D model of the Laurentide ice sheet Marshall and Clarke [44] first simulated such oscillations. Their sea level changes were small in comparison with recent proxy-data (about 10 m, [11]). Simulations of Heinrich events by [8] had an ice equivalent in sea level which matches well, with the finding by [11].

Like in the simulations of glacial inception in section 4.1 the simulations of Heinrich events are started at 126 kyr BP and run for 126,000 years through the whole glacial cycle using the same initial conditions as before. But in the simulation of Heinrich events the fact is accounted for that sliding over sediments is much faster than sliding over hard rock. By setting $m = 3$ and $l = 2$ for hard rock and $m = 1$ and $l = 0$ for soft sediment in (31) two different sliding laws follow:

$$\boldsymbol{v_H}(b) = \begin{cases} -C_{\mathrm{R}} H \parallel \boldsymbol{\nabla}_H^{r_0} h \parallel^2 \boldsymbol{\nabla}_H^{r_0} h & \text{for } T_{\mathrm{b}} = T_{\mathrm{pmp}} \text{ and hard rock,} \\ -C_{\mathrm{S}} H \boldsymbol{\nabla}_H^{r_0} h & \text{for } T_{\mathrm{b}} = T_{\mathrm{pmp}} \text{ and soft sediment,} \\ \mathbf{0} & \text{for } T_{\mathrm{b}} < T_{\mathrm{pmp}}, \end{cases} \quad (36)$$

with the basal temperature T_{b} and the pressure-melting temperature T_{pmp}. The sliding parameters for hard rock and soft sediment have the values $C_{\mathrm{R}} = 10^5\,\mathrm{a}^{-1}$ and $C_{\mathrm{S}} = 1000\,\mathrm{a}^{-1}$, respectively.

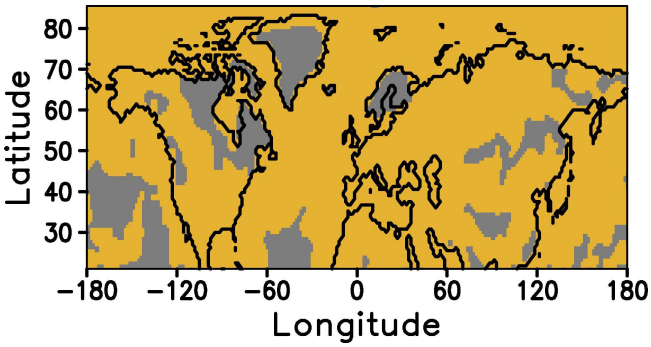

Fig. 6 Types of bedrock. Dark yellow indicates regions with soft sediment and grey shows regions with hard rock

The distribution of hard rock and soft sediment on the Northern Hemisphere (Fig. 6) is derived from global data of the sediment thickness [41]. It can be seen that Hudson Bay and Hudson Strait are not the only regions with soft sediment. There is soft sediment on the Canadian Archipelago and in the prairie in Northern America. These are regions where Heinrich events – or rather surging events, because the term Heinrich event stands exclusively for surging events over Hudson Bay and Hudson Strait – can appear potentially too. In Scandinavia, there is mainly hard rock surrounded by soft sediment. There is evidence of material in marine cores originating from these regions [28].

One pre-condition for Heinrich events is that the basal ice is at the melting point. Then, the question appears why broad basal regions of an ice sheet can nearly simultaneously reach the melting point. The onset of a Heinrich event was explained as a fast movement of a sharp gradient in the ice sheet elevation upstream of the Hudson Strait caused by an expansion of the temperate basal area starting at the mouth of Hudson Strait [8]. Such a mechanism is called activation wave [19]. This activation wave migrates far into Hudson Bay. The ice over Hudson Bay and Hudson Strait can move very fast now, because the basal ice is at the melting point enabling high sliding over the soft sediment. See [8] for details.

As noted before, the model is run through the whole glacial cycle. As observed [28] the simulated Heinrich events appear during the second half of the glacial cycle. Therefore, only results during that time span are presented here. Fig. 7 shows the surface elevation of the Laurentide ice sheet before and after a Heinrich event. The surface elevation of the Laurentide ice sheet dropped by about 1 km. The shape of the ice sheet changed substantially from a one-dome structure to a sickle-shaped structure.

In the simulations, Heinrich events obey the rules of chaos, i.e., with slightly different initial conditions the timing of the modelled events changes strongly. Fig. 8 shows two simulations which started at 65 kyr BP with slightly different initial conditions for the elevation of the Laurentide ice sheet. One initial condition in elevation was simply taken at 65 kyr BP; when the model computation was stopped, output was performed and the computation was continued with that initial condition. The other initial ice elevation, measured in meters, was produced with a random generator by multiplication of the factor $(1 - R \times 10^{-6})$, where $R \in (0, 1)$ is a random number, with the ice surface elevation at 65 kyr BP of the first Heinrich run. This factor produced a very small difference in elevation for the initial conditions at

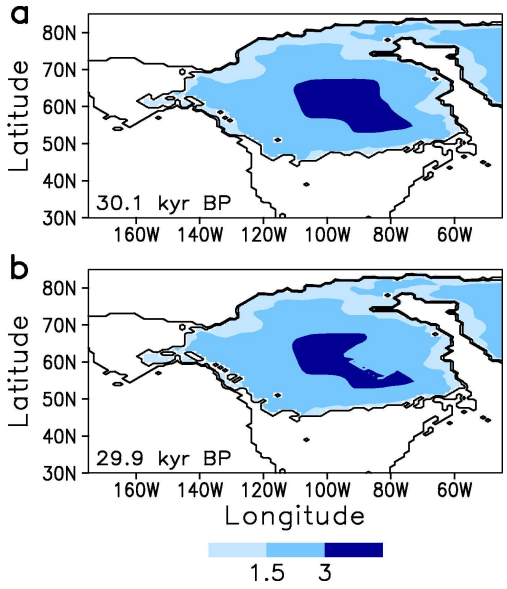

Fig. 7 Elevation of the Laurentide ice sheet in km (**a**) before and (**b**) after a Heinrich event

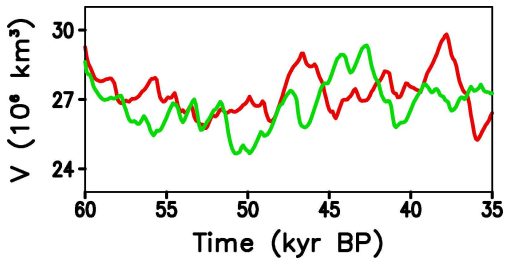

Fig. 8 Time series of ice volume of the Laurentide ice sheet in 10^6 km^3

65 kyr BP of the simulations. Nonetheless, one can see in Fig. 8 that the ice volume of the simulations immediately starts to deviate. These runs tell us that the timing of the Heinrich events as observed can only be simulated with a number of Monte-Carlo simulations. This also means that a single Heinrich event can never be reproduced in every detail.

5 Concluding Remarks

In this paper it was shown that thermomechanically coupled dynamics of land based ice sheets is governed by the creeping flow equations in the so-called shallow ice approximation, which, for climate modelling on the Earth, have been derived here in spherical coordinates. Such shallow ice equations are utilized for large-scale ice-sheet evolution in several contemporary ice sheet models, but in applications I used the polythermal variant SICOPOLIS, comprising

cold and temperate ice regions that are separated by a Stefan type transition surface. In the climate-system model CLIMBER-2, SICOPOLIS is one module in a coupled atmosphere-ocean-biosphere-cryosphere climate model of intermediate complexity, appropriate for time scales between 10 and 1,000,000 years. Application of SICOPOLIS within CLIMBER-2 demonstrated the importance of ice-sheet modelling in palaeo-climate research. This was done with two examples, the Last Glacial Inception and Heinrich events. The results showed that modelled ice sheet inception reproduced proxy-data in good agreement. The simulated Heinrich events corresponded to sea-level changes within the range of observations. But their chaotic response to initial conditions makes their detailed reproduction difficult.

I hope to have shown that palaeo-climate research is a challenging topic of mechanics and applied mathematics. The continuum mechanical approach, paired with sophisticated numerical techniques, proves to be important not only for the understanding of the mechanisms of the past climate change, it is equally also of help in forecast scenarios. The paper should also have provided a feeling how difficult it will be to reliably predict the reaction of the Earth's system to e.g. anthropogenic greenhouse scenarios. Reconstruction of the past climate is a prerequisite to achieve reliable predictions into the future.

Acknowledgements The author thanks Kolumban Hutter for the kind invitation to contribute this article to the GAMM-Mitteilungen and Andrey Ganopolski for the co-work and all the fruitful discussions. The comments and suggestions by Kolumban Hutter and Ralf Greve considerably improved an earlier version of the manuscript.

References

[1] J. M. Barnola, D. Raynaud, Y. S. Korotkevich, and C. Lorius, *Vostok ice core provides 160,000-year record of atmospheric CO_2*, Nature **329** (1987), 408–414.

[2] A. Berger and M. F. Loutre, *Astronomical theory of climate change*, Journal de Physique IV **121** (2004), 1–35.

[3] R. Bindschadler, *Future of the West Antarctic Ice Sheet*, Science **282** (1998), 428–429.

[4] G. Bond, W. Broecker, S. Johnsen, J. McManus, L. Labeyrle, J. Jouzel, and G. Bonani, *Correlations between climate records from North Atlantic sediments and Greenland Ice*, Nature **365** (1993), 143–147.

[5] V. Brovkin, J. Bendtsen, M. Claussen, A. Ganopolski, C. Kubatzki, C. V. Petoukhov, and A. Andreev, *Carbon cycle, vegetation, and climate dynamics in the Holocene: Experiments with the CLIMBER-2 model*, Glob. Biogeochem. Cyc. **16** (2002), 1139, doi: 10.1029/2001GB001662.

[6] R. Calov, A. Ganopolski, M. Claussen, V. Petoukhov, and R. Greve, *Transient simulation of the last glacial inception. Part I: glacial inception as a bifurcation of the climate system*, Climate Dyn. (2005a), doi: 10.1007/s00382-005-0007-6.

[7] R. Calov, A. Ganopolski, V. Petoukhov, M. Claussen, V. Brovkin, and C. Kubatzki, *Transient simulation of last glacial inception. Part II: sensitivity and feedback analysis*, Climate Dyn. (2005b), doi: 10.1007/s00382-005-0008-5.

[8] R. Calov, A. Ganopolski, V. Petoukhov, M. Claussen, and R. Greve, *Large-scale instabilities of the Laurentide ice sheet simulated in a fully coupled climate-system model*, Geophys. Res. Lett. **29** (2002), 2216, doi: 10.1029/2002GL016078.

[9] R. Calov and K. Hutter, *Large scale motion and temperature distributions in land based ice shields – the Greenland ice sheet in response to various climatic scenarios*, Arch. Mech. **49** (1997), 919–962.

[10] R. Calov, A. A. Savvin, R. Greve, I. Hansen, and K. Hutter, *Simulation of the Antarctic ice sheet with a three-dimensional polythermal ice-sheet model, in support of the EPICA project*, Ann. Glaciol. **27** (1998), 201–206.

[11] J. Chappell, *Sea level changes forced ice breakouts in the Last Glacial cycle: new results from coral terraces*, Quat. Sci. Rev. **21** (2002), 1229–1240.

[12] J. A. Church, J. M. Gregory, P. Huybrechts, M. Kuhn, K. Lambeck, M. T. Nhuan, D. Qin, and P. L. Woodworth, *Climate Change 2001: The Scientific Basis. Contribution of Working Group I to the Third Assessment Report of the Intergovernmental Panel on Climate Change*, pp. 639–693, Cambridge University Press, Cambridge etc., 2001.

[13] M. Claussen, A. Ganopolski, V. Brovkin, F.-W. Gerstengarbe, and P. Werner, *Simulated global-scale response of the climate system to Dansgaard-Oeschger and Heinrich events*, Climate Dyn. **21** (2003), 361–370.

[14] M. Claussen, L. A. Mysak, A. J. Weaver, M. Crucifix, T. Fichefet, M.-F. Loutre, S. L. Weber, J. Alcamo, V. A. Alexeev, A. Berger, R. Calov, A. Ganopolski, H. Goosse, G. Lohman, F. Lunkeit, I. I. Mokhov, V. Petoukhov, P. Stone, and Zh. Wang, *Earth system models of intermediate complexity: Closing the gap in the spectrum of climate system models*, Climate Dyn. **18** (2002), 579–586.

[15] W. Dansgaard, S. J. Johnsen, H. B. Clausen, D. Dahl-Jensen, N. S. Gundestrup, C. U. Hammer, C. S. Hvidberg, J. P. Steffensen, A. E. Sveinbjörnsdottir, J. Jouzel, and G. Bond, *Evidence for general instability of past climate from a 250-kyr ice-core record*, Nature **364** (1993), 218–220.

[16] R. F. Flint, *Glacial and Quaternary geology*, John Wiley and Sons, New York, London, Sydney, Toronto, 1971.

[17] P.-L. Forsström and R. Greve, *Simulation of the Eurasian ice sheet dynamics during the last glaciation*, Global Planet. Change **42** (2004), 59–81, doi: 10.1016/j.gloplacha.2003.11.003.

[18] P.-L. Forsström, O. Sallasmaa, R. Greve, T. Zwinger, *Simulation of fast-flow features of the Fennoscandian ice sheet during the Last Glacial Maximum*, Ann. Glaciol. **37** (2003), 383–389.

[19] A. C. Fowler and E. Schiavi, *A theory of ice-sheet surges*, J. Glaciol. **44** (1998), 104–118.

[20] A. Ganopolski, C. Kubatzki, M. Claussen, V. Brovkin, V. Petoukhov, *The influence of vegetation-atmosphere-ocean interaction on climate during the mid-Holocene*, Science **5371** (1998a), 1916–1919.
[21] A. Ganopolski, S. Rahmstorf, V. Petoukhov, and M. Claussen, *Simulation of modern and glacial climates with a coupled global climate model of intermediate complexity*, Nature **391** (1998b), 351–356.
[22] A. Ganopolski and S. Rahmstorf, *Rapid changes of glacial climate simulated in a coupled climate model*, Nature **409** (2002), 153–158.
[23] R. Greve *Thermomechanisches Verhalten polythermer Eisschilde – Theorie, Analytik, Numerik*, (Shaker Verlag, Aachen, Berichte aus der Geowissenschaft, 1995).
[24] R. Greve *A continuum-mechanical formulation for shallow polythermal ice sheets*, Phil. Trans. R. Soc. Lond. **A 355** (1997a), 921–974.
[25] R. Greve *Application of a polythermal three-dimensional ice sheet model to the Greenland ice sheet: Response to steady-state and transient climate scenarios*, J. Climate **10** (1997b), 901–918.
[26] R. Greve *On the response of the Greenland ice sheet to greenhouse climate change*, Climatic Change **46** (2000), 289–303.
[27] R. Greve and D. R. MacAyeal, *Dynamic/thermodynamic simulations of Laurentide ice-sheet instability*, Ann. Glaciol. **23** (1996), 328–335.
[28] F. E. Grousset C. Pujol, L. Labeyrie, G. Auffret, and A. Boelaert, *Were the North Atlantic Heinrich events triggered by the behavior of the European ice sheets?*, Geology **28** (2000), 123–126.
[29] H. Heinrich *Origin and consequences of cyclic ice rafting in the northeast Atlantic Ocean during the past 130,000 years*, Quat. Res. **29** (1988), 142–152.
[30] R. C. A. Hindmarsh and E. Le Meur, *Dynamical processes involved in the retreat of marine ice sheets*, J. Glaciol. **47** (2001), 271–282.
[31] K. Hutter, *Theoretical Glaciology; Material Science of Ice and the Mechanics of Glaciers and Ice Sheets*, (D. Reidel Publishing Company, Dordrecht, The Netherlands, 1983).
[32] K. Hutter and R. Calov, *Large scale motion and temperature distributions in land based ice shields – a review*, in: Proceedings of the 5th International Symposium on Thermal Engineering and Sciences for Cold Regions, Ottawa, Canada, 1996, edited by Y. Lee and W. Hallett (1996), 22–46.
[33] P. Huybrechts, *The Antarctic ice sheet and environmental change: a three-dimensional modelling study*, (Alfred Wegener Institute for Polar and Marine Research, Bremerhaven, Reports on Polar Research No. 99, 1992).
[34] P. Huybrechts, J. Gregory, I. Janssens, and M. Wild, *Modelling Antarctic and Greenland volume changes during the 20th and 21st centuries forced by GCM time slice integrations*, Global Planet. Change **42** (2004), 83–105.
[35] P. Huybrechts and J. Oerlemans, *Evolution of the East-Antarctic ice sheet: a numerical study on thermo-mechanical response patters with changing climate*, Ann. Glaciol. **11** (1988), 52–59.
[36] P. Huybrechts, D. Steinhage, F. Wilhelms, and J. Bamber, *Balance velocities and measured properties of the Antarctic ice sheet from a new compilation of gridded data for modelling*, Ann. Glaciol. **30** (2000), 52–60.
[37] P. Huybrechts and S. T'siobbel, *Thermomechanical modelling of northern hemisphere ice sheets with a two-level mass-balance parameterisation*, Ann. Glaciol. **21** (1995), 111–116.
[38] J. Imbrie, J. D. Hays, D. G. Martinson, A. McIntyre, A. C. Mix, J. J. Morley, N. G. Pisias, W. L. Prell, and N. J. Shackleton, *The orbital theory of Pleistocene climate: Support from a revised chronology of the marine $\delta^{18}O$ record*, in: Milankovitch and Climate, Part I, edited by A. Berger, J. Imbrie, J. Hays, G. Kukla, and B. Saltzman, (Reidel, Dordrecht, NATO ASI Series C: Mathematical and Physical Sciences 126, 1984), pp. 269–305.
[39] J. D. Ives, J. T. Andrews, and R. G. Barry, *Growth and decay of the Laurentide ice sheet and comparison with Fenno-Scandinavia*, Naturwissenschaften **62** (1975), 118–125.
[40] M. Kageyama, S. Charbit, C. Ritz, M. Khodri, and G. Ramstein, *Quatifiying ice-sheet feedbacks during the last glacial inception*, J. Geophys. Res. **31** (2004), L24203, doi: 10.1029/2004GL021339.

[41] G. Laske and G. A. Masters, *Global digital map of sediment thickness*, EOS trans. **AGU (78)** (1997), F483.
[42] A. Letréguilly, N. Reeh, and P. Huybrechts, *The Greenland ice sheet through the last glacial-interglacial cycle*, Global Planet. Change **90** (1991), 385–394.
[43] S. J. Marshall and G. K. C. Clarke, G. *A continuum mixture model of ice stream thermomechanics in the Laurentide ice sheet 1. Theorie*, J. Geophys. Res. **102** (1997a), 20599–20613.
[44] S. J. Marshall and G. K. C. Clarke, G. *A continuum mixture model of ice stream thermomechanics in the Laurentide ice sheet 2. Application to the Hudson Strait ice stream*, Journal **102** (1997b), 20615–20627.
[45] J. F. McManus, D. W. Oppo, and J. L. Cullen, *A 0.5-million-year record of millenial-scale climate variability in the North Atlantic*, Science **283** (1999), 971–975.
[46] M. Milankovitch, *Kanon der Erdbestrahlung und seine Anwendung auf das Eiszeitenproblem*, (Académie royale serbe, Édition speciale, Belgrade, 1941).
[47] L. W. Morland, *Thermo-mechanical balances of ice sheet flows*, Geophys. Astrophys. Fluid Dyn. **29** (1984), 237–266.
[48] F. Pattyn *A new three-dimensional higher-order thermomechanical ice-sheet model: basic sensitivity, ice-stream development and ice flow across subglacial lakes*, J. Geophys. Res. **108** (2003), 2382, doi:10.1029/2002JB002329.
[49] A. J. Payne, *Limit cycles in the basal thermal regime of ice sheets*, J. Geophys. Res. **100** (1995), 4249–4263.
[50] A. J. Payne and D. J. Baldwin, *Thermomechanical modelling of the Scandinavian ice sheet: implications for ice-stream formation*, Ann. Glaciol. **28** (1999), 83–89.
[51] A. J. Payne and P. W. Dongelmans, *Self-organization in the thermomechanical flow of ice sheets*, J. Geophys. Res. **102** (1997), 12,219–12,233.
[52] V. Petoukhov and A. Ganopolski, A set of climate models for integrated modelling of climate change impacts, Report 1-96, IIASA, Laxenburg, Austria (1994).
[53] C. Ritz, A. Fabré, and A. Letréguilly, *Sensitivity of a Greenland ice sheet model to ice flow and ablation parameters: consequences for the evolution through the last climatic cycle*, Climate Dyn. **13** (1997), 11–24.
[54] C. Ritz, V. Rommelaere, and C. Dumas, *Modeling the evolution of Antarctic ice sheet over the last 420,000 years: Implications for altitude changes in the Vostok region*, J. Geophys. Res. **106** (2001), 31,943–31,964.
[55] F. Saito, A. Abe-Ouchi, H. Blatter, *Effects of first-order stress gradients in an ice sheet evaluated by a three-dimensional thermomechanical coupled model*, Ann. Glaciol. **37** (2003), 166–172.
[56] T. F. Stocker, D. G. Wright, L. A. Mysak, *A zonally averaged, coupled ocean-atmosphere model for paleoclimate studies*, jclim **5** (1992), 773–797.
[57] L. Tarasov and W. R. Peltier, *Impact of thermomechanical ice sheet coupling on a model of the 100 kyr ice age cycle*, J. Geophys. Res. **104** (1999), 9517-9545.
[58] L. Tarasov and W. R. Peltier, *A geophysically constrained large ensemble analysis of the deglacial history of the North American ice-sheet complex*, Quat. Sci. Rev. **23** (2004), 359–388.
[59] C Waelbroeck, L. Labeyrie, E. Michel, J. C. Duplessy, J. F. McManus, K. Lambeck, E. Balbon, and M. Labracherie, *Sea-level and deep water temperature changes derived from benthic formaminifera isotopic records*, Quat. Sci. Rev. **21** (2002), 295–305.
[60] Z. Wang and L. A. Mysak, *Simulation of the last glacial inception and rapid ice sheet growth in the McGill Paleoclimate Model*, Geophys. Res. Lett. **29** (2002), 2102, doi: 10.1029/2002GL015120.
[61] J. Weertman, *Rate of growth or shrinkage of nonequilibrium ice sheets*, J. Glaciol. **5** (1964), 145–158.